Herschel Finds Evidence for Stellar Wind Particles in a Protostellar Envelope: Is This What Happened to the Young Sun?

Ceccarelli, C.; Dominik, C.; López-Sepulcre, A.; Kama, M.; Padovani, M.; Caux, E.; Caselli, P.

Link to publication

HERSCHEL FINDS EVIDENCE FOR STELLAR WIND PARTICLES IN A PROTOSTELLAR ENVELOPE: IS THIS WHAT HAPPENED TO THE YOUNG SUN?

C. Ceccarelli[1,2], C. Dominik[3,4], A. López-Sepulcre[1,2], M. Kama[3,5],
M. Padovani[6,7], E. Caux[8,9], and P. Caselli[10]

[1] Université Grenoble Alpes, IPAG, F-38000 Grenoble, France; Cecilia.Ceccarelli@obs.ujf-grenoble.fr
[2] CNRS, IPAG, F-38000 Grenoble, France
[3] Astronomical Institute Anton Pannekoek, University of Amsterdam, Postbus 94249, 1090-GE Amsterdam, The Netherlands
[4] Department of Astrophysics/IMAPP, Radboud University Nijmegen, 6525-AJ Nijmegen, The Netherlands
[5] Leiden Observatory, Leiden University, P.O. Box 9513, 2300-RA Leiden, The Netherlands
[6] Laboratoire Univers et Particules de Montpellier, UMR 5299 du CNRS, Université de Montpellier II,
cc072, F-34095 Montpellier, France
[7] INAF–Osservatorio Astrofisico di Arcetri, Largo E. Fermi 5, I-50125 Firenze, Italy
[8] Université de Toulouse, UPS-OMP, IRAP, F-31062 Toulouse, France
[9] CNRS, IRAP, 9 Av. Colonel Roche, BP 44346, F-31028 Toulouse Cedex 4, France
[10] School of Physics and Astronomy, University of Leeds, Leeds LS2 9JT, UK
Received 2014 February 28; accepted 2014 May 14; published 2014 July 1

ABSTRACT

There is evidence that the young Sun emitted a high flux of energetic ($\geqslant 10$ MeV) particles. The collisions of these particles with the material at the inner edge of the Protosolar Nebula disk induced spallation reactions that formed short-lived radionuclei, like ^{10}Be, whose trace is now visible in some meteorites. However, it is poorly known exactly when this happened, and whether and how it affected the solar system. Here, we present indirect evidence for an ejection of energetic particles in the young protostar, OMC-2 FIR 4, similar to that experienced by the young solar system. In this case, the energetic particles collide with the material in the protostellar envelope, enhancing the abundance of two molecular ions, HCO^+ and N_2H^+, whose presence is detected via *Herschel* observations. The flux of energetic particles at a distance of 1 AU from the emitting source, estimated from the measured abundance ratio of HCO^+ and N_2H^+, can easily account for the irradiation required by meteoritic observations. These new observations demonstrate that the ejection of $\geqslant 10$ MeV particles is a phenomenon occurring very early in the life of a protostar, before the disappearance of the envelope from which the future star accretes. The whole envelope is affected by the event, which sets constraints on the magnetic field geometry in the source and opens up the possibility that the spallation reactions are not limited to the inner edge of the Protosolar Nebula disk.

Key words: ISM: abundances – ISM: molecules – meteorites, meteors, meteoroids – stars: formation – stars: protostars

Online-only material: color figures

1. INTRODUCTION

The birth of a star is all but a peaceful process. Newborn stars emit X-rayfluxes thousands of times higher than those of the Sun (e.g., Feigelson & Montmerle 1999), UV photons are emitted by violent shocks caused by the gas falling onto the future star and matter is ejected at supersonic speeds in protostellar outflows. Finally, there is circumstantial evidence that the stellar winds of young forming stars accelerate nuclei at energies $\geqslant$ MeV, even in Sun-like stars (e.g., Feigelson et al. 2002b). The young Sun also exhibited these violent processes during its formation (e.g., Dauphas & Chaussidon 2011). One of the strongest proofs of this energetic start is the measured high initial over-abundance of short-lived (with half-lives of $\sim$1 My) radionuclides, whose decay products we can still find in meteorites today. For example, the calcium–aluminum-rich inclusions (CAIs) of carbonaceous meteorites contain ^{10}Be, with abundances larger than that found in the interstellar medium (ISM; e.g., Meyer & Clayton 2000; Chaussidon et al. 2006). The most accepted theory is that ^{10}Be has been produced by spallation reactions of solar wind nuclei with the quiescent gas at the inner edge of the solar nebula (McKeegan et al. 2000; Gounelle et al. 2001, 2006; Chaussidon & Gounelle 2007; Liu et al. 2010). The observed enrichment suggests doses of

about 10^{19}–10^{20} protons cm^{-2} (Gounelle et al. 2013). However, alternative theories attribute the measured ^{10}Be enrichment to Galactic cosmic rays (CRs; Desch et al. 2004) or to spallation reactions in the atmosphere of the young Sun and incorporated in the solar wind (Bricker & Caffee 2010).

Observations of young stars provide a crucial tool to understand the early history of the solar system (e.g., Caselli & Ceccarelli 2012). In particular, the detection of large fluxes of energetic particles in young protostars would provide support for the first theory and also help to constrain theories of particle acceleration in stellar winds. Unfortunately, it is practically impossible to directly detect high-energy stellar wind particles. The detection, therefore, must rely on indirect evidence. This detection is a problem similar to finding the astronomical objects where CRs, the $\geqslant$MeV particles pervading our Galaxy, are accelerated. In this case, the indirect detection is based on the effect that CRs have when they hit the H atoms of the ISM: (1) the creation of $\geqslant$GeV particles of π^0, which decay into detectable $\geqslant$GeV photons (Hayakawa 1952; Stecker 1971) and (2) the enhancement of ionization in the molecular gas irradiated by $\leqslant$GeV particles (Indriolo et al. 2010; Ceccarelli et al. 2011).

Since the expected $\geqslant$GeV photon flux from protostars is too low to be detected with present facilities, only the second method, the measurement of enhanced molecular gas ionization,
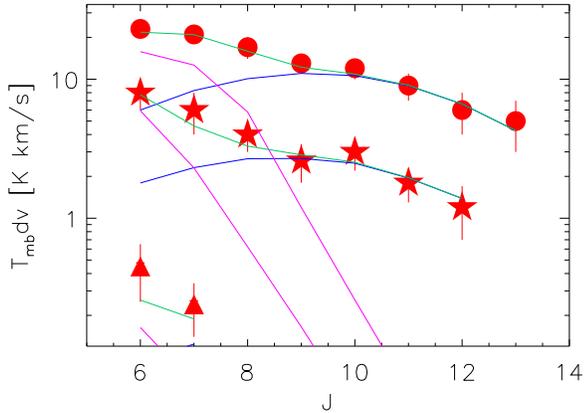
1

Figure 1. Spectral line energy distribution (SLED) of HCO$^+$ (circles), H^{13}CO$^+$ (triangles), and N$_2$H$^+$ (stars) as a function of the upper J transition. The curves show the intensities predicted by the adopted two-component model, the envelope (magenta) and warm (blue) component respectively (Table 1), and the sum of the two (green).

(A color version of this figure is available in the online journal.)

Figure 2. Dust density (blue) and temperature (red) profiles as derived from dust continuum emission (Crimier et al. 2009). The dashed boxes show the values derived in this work of the gas temperature and density, as determined by the LVG analysis for the envelope around 4000 AU and the warm component around 2000 AU, respectively. The stars show the two-component model adopted for the chemical and thermal analysis.

(A color version of this figure is available in the online journal.)

can be used to infer the presence of high-energy stellar wind particles in protostars. In Galactic molecular clouds, the molecular ionization is derived from the abundance ratio of DCO$^+$ over HCO$^+$ (Guélin et al. 1977; Caselli et al. 1998). However, this method, based on the enhanced DCO$^+$ abundance, only works for cold ($\leqslant$30 K) gas. Since the high-energy stellar wind particles will likely affect the innermost and warm regions of the envelope surrounding the new born star, this method cannot be used to measure the ionization caused by the energetic stellar wind particles.

As we will show in the following, the *Herschel Space Observatory* has provided us with a new probe of the ionization in the warm and dense gas: the abundance ratio of HCO$^+$ over N$_2$H$^+$ derived from highly excited rotational lines, whose upper level energy is $\geqslant$100 K.

2. THE DATA SET

The observations and analysis reported here refer to the source OMC-2 FIR 4, at a distance of 420 pc (Kim et al. 2008). Its mass and luminosity are around 30 $M_\odot$ (Mezger et al. 1990; Crimier et al. 2009) and $\lesssim$1000 $L_\odot$ (López-Sepulcre et al. 2013; Furlan et al. 2014 quote 100 $L_\odot$ for the FIR embedded protostar), respectively. OMC-2 FIR 4 contains a cluster of a few embedded intermediate and low-mass protostars (Shimajiri et al. 2008; López-Sepulcre et al. 2013).

We observed OMC-2 FIR 4 as part of the Key Program Chemical HErschel Surveys of Star forming regions (CHESS; Ceccarelli et al. 2010). The observations were obtained with the *Herschel* HIFI spectrometer (de Graauw et al. 2010) in 2010 and 2011. The survey covers the 480–1244 GHz frequency range with a spectral resolution of 1.1 MHz. The telescope beam size varies from 41 to 18 arcsec for the lowest to the largest frequencies. The data were reduced with the ESA HIPE v8 package (Ott 2010). The overall survey of OMC-2 FIR 4 and more details on the data reduction are presented in Kama et al. (2013).

Eight HCO$^+$, two H^{13}CO$^+$, and seven N$_2$H$^+$ lines are detected, all with upper level energies between $\sim$90 and 400 K, implying the presence of warm and dense gas (see Section 3.1 for a quantitative analysis). The observed spectral line energy distribution (SLED) is shown in Figure 1.
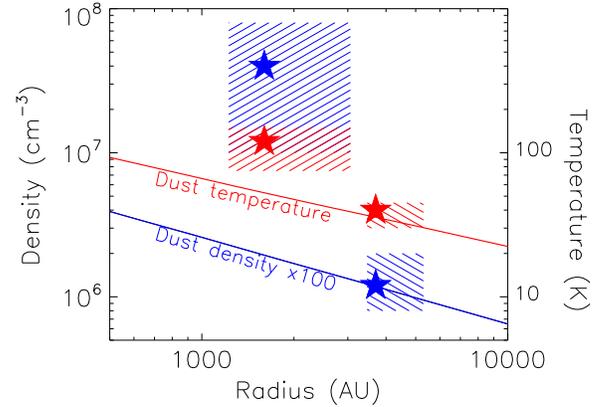
3. ANALYSIS

3.1. Physical Conditions and Column Densities

In order to derive the physical conditions of the emitting gas and the relevant column densities, we used the non-LTE large velocity gradient (LVG) code by Ceccarelli et al. (2003), with the collisional coefficients for HCO$^+$ with para-H$_2$ from Flower (1999), retrieved from the BASECOL database (http://basecol.obspm.fr/; Dubernet et al. 2013). Because the N$_2$H$^+$ collisional coefficients are not available, we used the same coefficients as those calculated for HCO$^+$, after scaling for the different molecular weight, because they have a similar electronic structure and molecular weight. In our calculations, we used these collisional coefficients for ortho-H$_2$ as well.

We ran a grid of models covering a large parameter space in temperature (from 25 to 150 K), H$_2$ density (from 6×10^5 to 1×10^9 cm^{-3}), HCO$^+$ and N$_2$H$^+$ column density (from 1×10^{13} to 2×10^{15} cm^{-2}), and source size (0.1–200 arcsec).

Crimier et al. (2009) modeled the dust continuum emission of the outer envelope of OMC-2 FIR 4 and derived the temperature and density profiles shown in Figure 2. Using this model, we failed to reproduce the observed SLEDs. While the lower J lines can be reproduced, the higher J lines cannot. Therefore, we modeled the SLED of HCO$^+$, H^{13}CO$^+$, and N$_2$H$^+$ simultaneously, assuming that the emission originates from two components, one of which is the cold outer envelope, and the other a warmer, denser envelope. Our aim is to estimate the average density, temperature, size, and HCO$^+$ and N$_2$H$^+$ abundances in the second component. Since HCO$^+$ and N$_2$H$^+$ share a very similar molecular structure, chemical origin (Section 3.2), and excitation mechanisms, it is highly likely that they are located in the same regions—which we will assume in the following. Some general considerations help to constrain the explored parameter space. First, the HCO$^+$ lines are likely only moderately optically thick, as the HCO$^+$ over H^{13}CO$^+$ line intensity ratio is $\sim$30, slightly smaller than the standard ^{12}C/^{13}C ratio ($\sim$75; Wilson & Rood 1994). Second, the HCO$^+$ over N$_2$H$^+$ line intensity ratio is between 3 and 5. Therefore, we considered the [HCO$^+$]/[N$_2$H$^+$] abundance ratio between 3 and 10.

We found acceptable solutions ($\chi^2_{\rm red} \leqslant 1$) for two components with [HCO$^+$]/[N$_2$H$^+$] between three and four and the following

Table 1
Parameters of the Gas Emitting HCO^+ and N_2H^+, as Derived from the
Non-LTE LVG (Top) and Chemical (Bottom) Analysis

	Warm Component		Envelope	
	Adopted Solution[a]	Range	Adopted Solution[a]	Range
Results from the non-LTE LVG analysis				
H_2 density (cm^{-3})	4.0×10^7	$1–80 \times 10^7$	1.2×10^6	$0.8–2 \times 10^6$
Temperature (K)	120	75–150	40	30–45
Source size (arcsec)	8	6–15	18	17–26
Source radius (AU)	1600	1250–3000	3700	3500–5000
$N(HCO^+)$ (cm^{-2})	7×10^{13}	$6–15 \times 10^{13}$	3×10^{14}	$2–6 \times 10^{14}$
$N(N_2H^+)$ (cm^{-2})	3×10^{13}	$2–5 \times 10^{13}$	1×10^{14}	$0.5–2 \times 10^{14}$
HCO^+/N_2H^+	3.5	3–4	3.5	3–4
Results from the chemistry analysis				
CR ion. rate ζ (s^{-1})	6×10^{-12}	$\geqslant 1.5 \times 10^{-12}$	4×10^{-14}	$1.5–8 \times 10^{-14}$
$x(HCO^+)$[b]	1×10^{-7}	$\geqslant 2 \times 10^{-8}$	6×10^{-8}	$4–10 \times 10^{-8}$
$x(N_2H^+)$[b]	3×10^{-8}	$\geqslant 6 \times 10^{-9}$	2×10^{-8}	$1–3 \times 10^{-8}$

Notes. The parameter range is obtained considering solutions with $\chi^2_{\mathrm{red}} \leqslant 1$ equivalent to a 1σ level of confidence.
[a] Parameters of the model adopted for the chemistry and thermal analysis.
[b] Abundances with respect to H_2.

properties: (1) a first component whose temperature and density are 30–45 K and $0.8–2 \times 10^6$ cm^{-3}, respectively, namely those of the envelope at radii between 3500 and 5000 AU (Figure 2); (2) a second component whose temperature and density are 75–150 K and $1–80 \times 10^7$ cm^{-3}, and relatively compact, 6–14 arcsec, equivalent to a radius of 1250–3000 AU. Table 1 lists the parameters of the solution adopted for the chemical analysis and the range of permitted values. The predicted SLED of the adopted solution is plotted in Figure 1, together with the observations. Figure 2 shows the density and temperature of the gas derived from the LVG analysis, compared with the envelope profiles.

3.2. Chemistry

The most remarkable result from the previous analysis is the low value of $[HCO^+]/[N_2H^+] \sim 3–4$, much lower than that expected in similar astrophysical environments (Figure 3). This value is close to the elemental abundance ratio of C/N, two elements that are present in molecular clouds mostly in the form of CO and N_2.

The main chemical pathway to the *formation* of HCO^+ and N_2H^+ is the reaction of CO and N_2, respectively, with H_3^+, an ion created from the ionization of H_2 by CR:

$$CO\ (N_2) + H_3^+ \rightarrow HCO^+\ (N_2H^+) + H_2.$$

Since the production mechanism of both molecules is the same, the reason why the $[HCO^+]/[N_2H^+]$ abundance ratio is normally much larger than three lies in the chemical reactions that lead to the *destruction* of these molecules. Usually CO, being the most abundant neutral, is the main destroyer. When a neutral CO molecule collides with N_2H^+, the product is HCO^+ (e.g., Bergin & Langer 1997). The way to lower $[HCO^+]/[N_2H^+]$ is, therefore, either to lower the CO abundance ($\lesssim 10^{-5}$) and not the N_2 or to introduce a destruction channel that acts symmetrically on both molecules. The previous analysis shows that the HCO^+ emission originates in warm regions, where CO is unlikely trapped in CO ices. Some carbon may be trapped in less volatile CO_2 ices. However, using the Furlan et al. (2014) spectrum toward OMC-2 FIR 4, we estimate a CO_2 abundance of $\sim 5 \times 10^{-6}$. Therefore, a low CO abundance
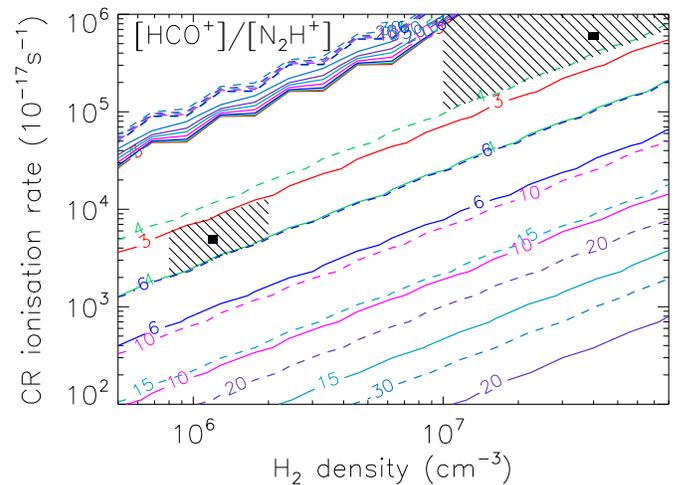

Figure 3. Theoretical $[HCO^+]/[N_2H^+]$ abundance ratio for a gas temperature of 40 K (solid lines) and 120 K (dashed lines) as a function of the density and CR ionization rate ζ. The hashed boxes mark the range of density and ζ of the envelope and warm components, the black squares mark the adopted solution values. The plot has been obtained with the code ASTROCHEM (http://smaret.github.com/astrochem/), the OSU2009 chemical network and the following elemental abundances (with respect to H nuclei): nitrogen 2.1×10^{-5}, carbon 7.3×10^{-5}, and oxygen 1.8×10^{-4}. The figure shows that, for standard ζ ($\leqslant 10^{-16}$ s^{-1}), the predicted $[HCO^+]/[N_2H^+]$ is $\geqslant 10$ for densities $\geqslant 5 \times 10^5$ cm^{-2}, and close to three only for large ζ. Note that very high values of ζ cause the gas to flip from the low ionization phase (LIP) to the high ionization phase (HIP; Pineau des Forets et al. 1992). In the HIP (degenerate solutions in the upper part of the plot), both HCO^+ and N_2H^+ have extremely low abundances, about 10^3 times lower than in the LIP. Therefore, if HCO^+ and N_2H^+ are detected, they very likely originate in the LIP (lower part of the plot) and there is no problem of degeneracy in linking the measured $[HCO^+]/[N_2H^+]$ ratio to ζ.
(A color version of this figure is available in the online journal.)

hypothesis cannot work. Candidates for a symmetric destroyer channel are reactions with neutral molecules whose abundance is $\geqslant 10^{-5}$, or electrons.

The only neutral molecule candidate is H_2O. However, in both components the dust and gas temperatures are too low to produce a sufficiently large H_2O abundance (by ice sublimation and gas phase reactions) (Figure 2). To verify this, we analyzed the H_2O lines in the CHESS spectrum. Although the H_2O lines are much broader (~ 20 km s^{-1}) than the HCO^+ and N_2H^+ lines ($\leqslant 5$ km s^{-1}), implying that they do not originate in the same gas, we can use them for a sanity check, to give an upper limit to the water abundance in the envelope and warm component, respectively. To this end, we ran LVG models, using the parameters in Table 1. We find that the water abundance is $\leqslant 10^{-6}$, confirming that the major destroyer of HCO^+ and N_2H^+ cannot be water molecules.

The only alternative destroyer of HCO^+ and N_2H^+ are, therefore, free electrons. The question is what could cause a large electron abundance. In principle, there are three possibilities: UV radiation, X-rays, and accelerated $\geqslant$MeV particles, namely CR-like particles (for simplicity, we will call them CR). UV photons can be ruled out, as they would destroy H_3^+ (whose rate of formation is only given by the CR flux) and, consequently inhibit the production of HCO^+ and N_2H^+. To verify this, we ran the Meudon photodissociation region (PDR) code (http://pdr.obspm.fr/PDRcode.html; Le Petit et al. 2006) and found that, as expected, $[HCO^+]/[N_2H^+] \geqslant 10^3$ in the PDR. X-ray irradiation does increase the electron abundance by ionizing H_2 molecules and creating the H_3^+ ions, similarly to what happens to CR irradiated molecular gas

(e.g., Maloney et al. 1996; Meijerink et al. 2006). However, *Chandra* X-ray observations of the region did not detect emission from OMC-2 FIR 4, therefore putting an upper limit to the X-ray flux in the energy range from 0.5 to 8 keV of 4×10^{-16} erg cm^{-2} s^{-1} (Feigelson et al. 2002a). For a source at a distance of 420 pc, this implies a limit on the luminosity emerging from the protostar of $\leqslant 8 \times 10^{27}$ erg s^{-1}. Translating this into an X-ray source luminosity requires assumptions of the column density and the shape of the X-ray spectrum. We follow the formalism by Maloney et al. (1996). Using a hydrogen column density of 2×10^{23} cm^{-2} (Crimier et al. 2009), the observed luminosity limit translates into an X-ray luminosity limit of the central source of 0.03–70×10^{30} erg s^{-1} for an X-ray spectrum that is flat or $\propto E^{-3}$, respectively. In either case, the resulting limit for the X-ray ionization rate in the envelope at 3700 AU is $\sim 1.5 \times 10^{-20}$ s^{-1}, too small to explain the ionization rate probed by our observations. This result is very robust because it is a direct consequence of the observed X-ray limit and rather independent of assumptions about the intrinsic X-ray spectrum. The same X-ray luminosity could lead to higher rates closer to the emitting source if the attenuating column is significantly lower. Therefore, while an X-ray contribution in the warm component is possible, it is firmly excluded in the cold component.

In conclusion, the observed small [HCO$^+$]/[N$_2$H$^+$] ratio is due to a strongly enhanced flux of CR-like particles. In Figure 3, we plot [HCO$^+$]/[N$_2$H$^+$] at different densities and CR ionization rates, ζ, for a gas at temperatures of 40 and 120 K, respectively (Table 1). Comparison between observations and model predictions provide us with constraints on ζ: 1.5–8×10^{-14} and $\geqslant 1.5 \times 10^{-12}$ s^{-1} in the envelope and warm component, respectively.

3.3. Thermal Balance

In addition to ionizing the molecular gas, CR also heats it. We can, therefore, further examine the hypothesis of CR irradiation by computing the gas temperature, assuming that the gas is heated by the CR and cooled by the dust–gas collisions and line emission. For the CR heating we used the results by Glassgold et al. (2012), for the cooling we adopted the formalism described in Ceccarelli et al. (1996) and considered the contributions of CO and H$_2$O molecules, and atomic oxygen. The H$_2$O abundance was computed assuming equilibrium between freeze-out on grains, and desorption triggered by CR, following the formalism of Hasegawa & Herbst (1993) and Dominik et al. (2006). We obtained a water abundance of 1.5×10^{-8} and 9×10^{-9} in the warm component and envelope, respectively. Atomic oxygen was added to the mix with an assumed abundance of 10^{-5}. We ran the thermal balance model for the range of densities and ζ given in Table 1. We obtained that the gas temperature is roughly equal to that of the dust in the cold envelope and about 70 K larger in the warm component, in agreement with the gas temperatures derived by the LVG analysis (Figure 2). In the envelope, the cooling is dominated by the CO emission, whereas, in the warm component, it is equally shared between dust–gas collisions and CO line emission.

3.4. Energetic Particle Flux

The analysis of the two previous subsections provides compelling evidence for the presence of a source of CR-like particles inside the OMC-2 FIR 4 envelope, as the inner warm component is the one with the higher ionization rate. Of particular relevance here is the flux of particles with $E \geqslant 10$ MeV, as they can form
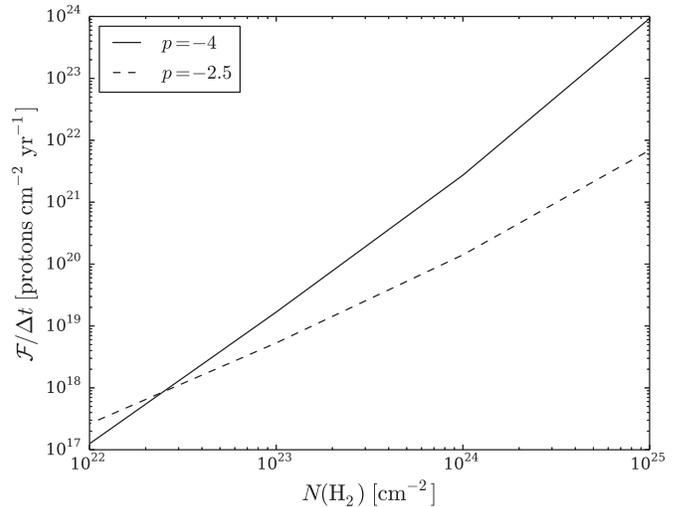

Figure 4. Flux of $\geqslant 10$ MeV particles as a function of the column density between the emitting source and 3700 AU, for an input energy spectrum $f(E) \propto E^p$ with $p = -4$ (solid line) and -2.5 (dashed line).

^{10}Be by spallation reactions (Sisterson et al. 1997; Lange et al. 1995; Gounelle et al. 2006), and how it compares with the fluence estimated for the ^{10}Be meteoritic enrichment: ~ 2–30×10^{19} protons cm^{-2} (Gounelle et al. 2013). The underlining hypothesis is that the young Sun underwent flares, similar to those observed in YSOs (e.g., Lee et al. 1998; Feigelson et al. 2002b).

In order to estimate the $E \geqslant 10$ MeV particle fluence, we need to know the emitted particle energy spectrum. We derived it from the measured ζ at 3700 AU (Table 1) as follows. We first assumed an input particle energy spectrum and computed ζ at 3700 AU, taking into account the geometric dilution and attenuation caused by the material between the source and 3700 AU. Then, we scaled the input particle energy spectrum so that the measured ζ at 3700 AU is reproduced. Finally, we computed the $E \geqslant 10$ MeV particle flux at, for example, a distance of 1 AU, assuming that there is no attenuation on this scale.

Following Gounelle et al. (2001), we assumed a 0.1–100 MeV input particle energy spectrum $f(E) \propto E^p$, with p varying between -4 and -2.5. To compute the attenuation, we used the formalism described in Padovani et al. (2009). Since the column density between the emitting source and 3700 AU is uncertain (1.5×10^{23} cm^{-2} according to the Crimier et al. 2009 model), we consider it a variable of the model. The results of these computations are shown in Figure 4. We found that for a column density of 1.5×10^{23} cm^{-2} the flux is ~ 1–3×10^{19} protons cm^{-2} yr^{-1}. Therefore, an irradiation time of a few years at 1 AU (or correspondingly longer at larger distances) would easily account for the fluence derived by Gounelle et al. (2013). We are aware that we ignore effects of magnetic fields on the propagation of energetic particles, such as (partial) confinement (Gounelle et al. 2001) and path distortions that increase the attenuation columns (Padovani et al. 2013). Quantifying these effects would require knowledge of the magnetic field in the region. However, our simple calculations suggest an $E \geqslant 10$ MeV particle flux similar to, if not larger than, that of the young Sun.

4. CONCLUSIONS

We presented the analysis of the HCO$^+$ and N$_2$H$^+$ SLED, observed by the *Herschel* HIFI CHESS Key Program toward

the protostar OMC-2 FIR 4. The comparison with a non-LVG model shows the presence of a warm ($\sim$120 K) and dense ($\sim 4 \times 10^7$ cm^{-3}) component, in addition to the envelope ($\sim$40 K and $\sim 1 \times 10^6$ cm^{-3}) probed by continuum observations (Crimier et al. 2009).

The most remarkable and important result of this work is the derived low [HCO$^+$]/[N$_2$H$^+$] abundance ratio: $\sim$3–4. We showed that this suggests the presence of a large flux of CR-like particles inside the envelope, with a ionization rate of 1.5–8 $\times 10^{-14}$ and $\geqslant 1.5 \times 10^{-12}$ s^{-1} in the envelope and warm component, respectively.

The estimated flux of $E \geqslant 10$ MeV particles at 1 AU distance from the emitting source, $\geqslant$1–3 $\times 10^{19}$ protons cm^{-2} yr^{-1}, is more than that recorded in the ^{10}Be of meteoritic material assuming flare times of a few years.

The present observations support the theory that meteoritic ^{10}Be was formed in situ by spallation reactions, rather than moved from the solar atmosphere (Section 1). They also show that young protostars still embedded in their placental envelope can be sites of energetic particle ejections, as indirectly suggested for the young Sun by the recent analysis of ^{10}Be in CAI 411 (Gounelle et al. 2013). These particles affect the entire envelope, and not only the circumstellar disk, providing constraints on the magnetic field structure. These findings will certainly have an impact on the present theories of the energetic particle acceleration in the young solar system as well as on the magnetic field geometry in protoclusters.

REFERENCES

Bergin, E. A., & Langer, W. D. 1997, ApJ, 486, 316
Bricker, G. E., & Caffee, M. W. 2010, ApJ, 725, 443
Caselli, P., & Ceccarelli, C. 2012, A&ARv, 20, 56
Caselli, P., Walmsley, C. M., Terzieva, R., & Herbst, E. 1998, ApJ, 499, 234
Ceccarelli, C., Bacmann, A., Boogert, A., et al. 2010, A&A, 518, L22
Ceccarelli, C., Hily-Blant, P., Dubus, G., et al. 2011, ApJL, 740, L4
Ceccarelli, C., Hollenbach, D. J., & Tielens, A. G. G. M. 1996, ApJ, 471, 400
Ceccarelli, C., Maret, S., Tielens, A. G. G. M., Castets, A., & Caux, E. 2003, A&A, 410, 587
Chaussidon, M., & Gounelle, M. 2007, CRGeo, 339, 827
Chaussidon, M., Robert, F., & McKeegan, K. D. 2006, GeCoA, 70, 224
Crimier, N., Ceccarelli, C., Lefloch, B., & Faure, A. 2009, A&A, 506, 1229
Dauphas, N., & Chaussidon, M. 2011, AREPS, 39, 351
de Graauw, T., Helmich, F. P., Phillips, T. G., et al. 2010, A&A, 518, L6
Desch, S. J., Connolly, H. C., Jr., & Srinivasan, G. 2004, ApJ, 602, 528
Dominik, C., Ceccarelli, C., Hollenbach, D. J., & Kaufman, M. 2006, ApJL, 635, L85
Dubernet, M.-L., Alexander, M. H., Ba, Y. A., et al. 2013, A&A, 553, 50
Feigelson, E. D., Broos, P., Gaffney, J. A., III, et al. 2002a, ApJ, 574, 258
Feigelson, E. D., Garmire, G. P., & Pravdo, S. H. 2002b, ApJ, 572, 335
Feigelson, E. D., & Montmerle, T. 1999, ARA&A, 37, 363
Flower, D. R. 1999, MNRAS, 305, 651
Furlan, E., Megeath, S. T., Osorio, M., et al. 2014, ApJ, 786, 26
Glassgold, A. E., Galli, D., & Padovani, M. 2012, ApJ, 756, 157
Gounelle, M., Chaussidon, M., & Rollion-Bard, C. 2013, ApJL, 763, L33
Gounelle, M., Shu, F. H., Shang, H., et al. 2001, ApJ, 548, 1051
Gounelle, M., Shu, F. H., Shang, H., et al. 2006, ApJ, 640, 1163
Guélin, M., Langer, W. D., Snell, R. L., & Wootten, H. A. 1977, ApJL, 217, L165
Hasegawa, T. I., & Herbst, E. 1993, MNRAS, 261, 83
Hayakawa, S. 1952, PThPh, 8, 571
Indriolo, N., Blake, G. A., Goto, M., et al. 2010, ApJ, 724, 1357
Kama, M., López-Sepulcre, A., Dominik, C., et al. 2013, A&A, 556, 57
Kim, M. K., Hirota, T., Honma, M., et al. 2008, PASJ, 60, 991
Lange, H.-J., Hahn, T., Michel, R., et al. 1995, Appl. Radiat. Isot., 46, 83
Lee, T., Shu, F. H., Shang, H., Glassgold, A. E., & Rehm, K. E. 1998, ApJ, 506, 898
Le Petit, F., Nehmé, C., Le Bourlot, J., & Roueff, E. 2006, ApJS, 164, 506
Liu, M.-C., Nittler, L. R., Alexander, C. M. O., & Lee, T. 2010, ApJL, 719, L99
López-Sepulcre, A., Taquet, V., Sánchez-Monge, Á., et al. 2013, A&A, 556, 62
Maloney, P. R., Hollenbach, D. J., & Tielens, A. G. G. M. 1996, ApJ, 466, 561
McKeegan, K. D., Chaussidon, M., & Robert, F. 2000, Sci, 289, 1334
Meijerink, R., Spaans, M., & Israel, F. P. 2006, ApJL, 650, L103
Meyer, B. S., & Clayton, D. D. 2000, SSRv, 92, 133
Mezger, P. G., Zylka, R., & Wink, J. E. 1990, A&A, 228, 95
Ott, S. 2010, in ASP Conf. Ser. 434, Astronomical Data Analysis Software and Systems XIX, ed. Y. Mizumoto, K.-I. Morita, & M. Ohishi (San Francisco, CA: ASP), 139
Padovani, M., Galli, D., & Glassgold, A. E. 2009, A&A, 501, 619
Padovani, M., Hennebelle, P., & Galli, D. 2013, A&A, 560, 114
Pineau des Forets, G., Roueff, E., & Flower, D. R. 1992, MNRAS, 258, 45
Shimajiri, Y., Takahashi, S., Takakuwa, S., Saito, M., & Kawabe, R. 2008, ApJ, 683, 255
Sisterson, J. M., Kim, M., Caffee, M. W., & Reedy, R. C. 1997, LPSC, 28, 1327
Stecker, F. W. 1971, Natur, 234, 28
Wilson, T. L., & Rood, R. 1994, ARA&A, 32, 191